RESEARCH LETTER

Key Points:
- Regional surface warming is consistent with changed TOA energy balance
- Interactions between components of energy balance hinder attribution
- Energy transport leads to nonlocal effects from uncertain processes

Correspondence to:
T. M. Merlis,
timothy.merlis@mcgill.ca

Interacting components of the top-of-atmosphere energy balance affect changes in regional surface temperature

Timothy M. Merlis[1]

[1]Department of Atmospheric and Oceanic Sciences, McGill University, Montreal, Quebec, Canada

Abstract The role of interactions between components of the top-of-atmosphere (TOA) energy balance in determining regional surface temperature changes, such as polar amplification, is examined in diffusive energy balance model (EBM) simulations. These interactions have implications for the interpretation of local feedback analyses when they are applied to regional surface temperature changes. Local feedback analysis succeeds at accounting for the EBM-simulated temperature change given the changes in the radiative forcing, atmospheric energy transport, and radiative feedbacks. However, the inferences about the effect of individual components of the TOA energy balance on regional temperature changes do not account for EBM simulations in which individual components are prescribed or "locked." As changes in one component of the TOA energy balance affect others, unambiguous attribution statements relating changes in regional temperature or its intermodel spread to individual terms in the TOA energy balance cannot be made.

1. Introduction

The climate's top-of-atmosphere (TOA) energy balance is central in determining the surface temperature response to radiative forcing agents. In the global mean, the magnitude of the surface temperature response is determined by the combined effect of changes in energy storage and radiative feedbacks arising from changes in radiatively active climate constituents (e.g., sea ice and atmospheric water vapor). For regional surface temperature changes, one must consider changes in the energy transport by the atmosphere and ocean as well as the spatial structure of the radiative forcing, radiative feedbacks, and energy storage rate.

In recent work, authors have made use of local descriptions of the climate's perturbation TOA energy balance to attribute regional changes in surface temperature to individual components of it, such as the geographic pattern of radiative feedbacks or atmospheric energy transport [*Winton*, 2006; *Lu and Cai*, 2009; *Crook et al.*, 2011; *Kay et al.*, 2012; *Feldl and Roe*, 2013; *Taylor et al.*, 2013; *Pithan and Mauritsen*, 2014]. The perturbation TOA energy balance is approximately linear in these components, so authors have decomposed regional surface temperature changes, such as the degree of polar or Arctic amplification and the intermodel spread of these changes into fractional contributions associated with the individual components of the TOA energy balance (section 2.1). However, underlying the linearity of the TOA energy balance are interactions between the different components of the energy balance. In this letter, I present an example of such interactions in a simple climate model—a diffusive energy balance model (EBM).

Here EBM simulations with interactive surface albedo feedback and atmospheric energy transport are compared to EBM simulations in which changes in one of these components of the TOA energy balance are prescribed (this is often referred to as a "feedback-locking" simulation [e.g., *Schneider et al.*, 1999]). Comparing the simulations with interactive components to those with locked components reveals that interactions between the processes affecting the TOA energy balance are important. Spatially confined feedbacks influence energy transport and therefore nonlocally affect temperature. The energy transport, in turn, modifies the structure and magnitude of radiative feedbacks. This suggests that the meaning of attribution statements for regional temperature changes that are made using the local TOA energy balance is ambiguous: one cannot infer what the local change would be in the *absence* of that associated with a particular component of the TOA energy balance, as the other components may change differently. The discussion is centered on polar amplification, as this has been a focus of several publications; however, the issue raised is general.

The appeal of examining a diffusive EBM is that it is straightforward to interpret: this is the simplest climate model with interactions between localized radiative feedbacks and the atmospheric energy transport. In addition, it is less technically demanding to lock feedbacks in an EBM than in a general circulation model (GCM), and the complicating factors of time fluctuations and correlations between variables in GCM feedback-locking simulations [e.g., *Schneider et al.*, 1999] are not present in the EBM. Last, the atmospheric energy transport can readily be prescribed in the EBM [see also *Alexeev and Jackson*, 2013]. These advantages come at the expense of having a less close connection to more comprehensive climate models, to which the TOA energy balance analysis is typically applied. The EBM results are placed in the context of published GCM simulations with locked feedbacks in the final section.

2. Methods

2.1. TOA Energy Balance Surface Temperature Analysis

The spatially varying, perturbation (indicated by Δ) TOA energy balance is $\Delta\mathcal{H} = \Delta N_{TOA} - \Delta(\nabla \cdot \mathbf{F})$, with energy storage rate $\mathcal{H}$, TOA net radiation N_{TOA}, and the mass-weighted vertically integrated sum of atmosphere and ocean energy transport $\mathbf{F}$. The change TOA net radiation ΔN_{TOA} can be written as the sum of radiative forcing $\mathcal{F}$ and the sum of the radiative feedbacks $\Sigma_i \lambda_i \Delta T_s$, with climate feedback parameters λ_i and surface temperature T_s. Only equilibrium climates states are considered in what follows ($\Delta\mathcal{H} = 0$), though the analysis can be applied to transient climate states. With these definitions, the equilibrium perturbation TOA energy balance is

$$\mathcal{F} + \lambda_P \Delta T_s + \sum_{j \neq P} \lambda_j \Delta T_s = \Delta(\nabla \cdot \mathbf{F}), \qquad (1)$$

where the Planck feedback λ_P has been separated from the other feedbacks (water vapor, lapse rate, surface albedo, and cloud feedbacks in the conventional decomposition).

Using latitude ϕ to denote that this is a local form of the TOA energy balance, (1) can be rearranged to isolate the local surface temperature change:

$$\Delta T_s(\phi) = \left\{ -\mathcal{F}(\phi) + \Delta[\nabla \cdot \mathbf{F}(\phi)] - \sum_{j \neq P} \lambda_j(\phi) \Delta T_s(\phi) \right\} \times \lambda_P(\phi)^{-1}. \qquad (2)$$

This form of the TOA energy balance has been used to make inferences about regional changes in surface temperature $\Delta T_s(\phi)$ in terms of changes appearing on the right-hand side of (2): the radiative forcing, changes in the atmospheric and oceanic energy transport, the non-Planck radiative feedbacks, and the meridional structure of the Planck feedback [e.g., *Winton*, 2006; *Crook et al.*, 2011; *Feldl and Roe*, 2013]. In deriving (2), standard assumptions of climate feedback analysis, such as the neglecting radiation changes that depend nonlinearly on the surface temperature change, are used [e.g., *Feldl and Roe*, 2013].

2.2. Diffusive EBM

The TOA energy balance surface temperature analysis (2) is performed on the simplest climate model with an interactive representation of the atmospheric energy transport and radiative feedbacks—a diffusive energy balance model (EBM) with temperature-dependent surface albedo. The governing equation of the one-dimensional, diffusive EBM follows *Sellers* [1969] and *North et al.* [1981]:

$$c_p \partial_t T_s = \frac{1}{4} QS[1 - \alpha(T_s)] + A + BT_s - \nabla \cdot \mathbf{F_a} + \mathcal{F}, \qquad (3)$$

with heat capacity c_p, solar constant Q, meridional insolation structure function S, surface albedo $\alpha(T_s)$, outgoing longwave radiation $-(A + BT_s)$, divergence of the atmospheric energy transport $\nabla \cdot \mathbf{F_a}$, and radiative forcing $\mathcal{F}$. The divergence of the atmospheric energy transport is represented by diffusing surface temperature $\nabla \cdot \mathbf{F_a} = -\partial_x \left[D(1 - x^2)\partial_x T_s \right]$, with $x = \sin\phi$. The results presented here use the following temperature-dependent form of the surface albedo

$$\alpha(T_s) = \frac{\alpha_o + \alpha_i}{2} + \frac{\alpha_o - \alpha_i}{2} \tanh\left(\frac{T_s - T_0}{h_T}\right). \qquad (4)$$

The default parameter values are $Q = 1360$ W m^{-2}, $S = 1 - 0.482(3x^2 - 1)/2$, $c_p = 2 \times 10^8$ J °C^{-1}, $A = -200$ W m^{-2}, $B = -1.75$ W m^{-2} °C^{-1}, $D = 0.3$ W m^{-2} °C^{-1}, $\alpha_o = 0.32$, $\alpha_i = 0.62$, $T_0 = -11$°C, and $h_T = 6$°C. The sign convention for A, B, and (3) is consistent with the convention that the Planck feedback is negative
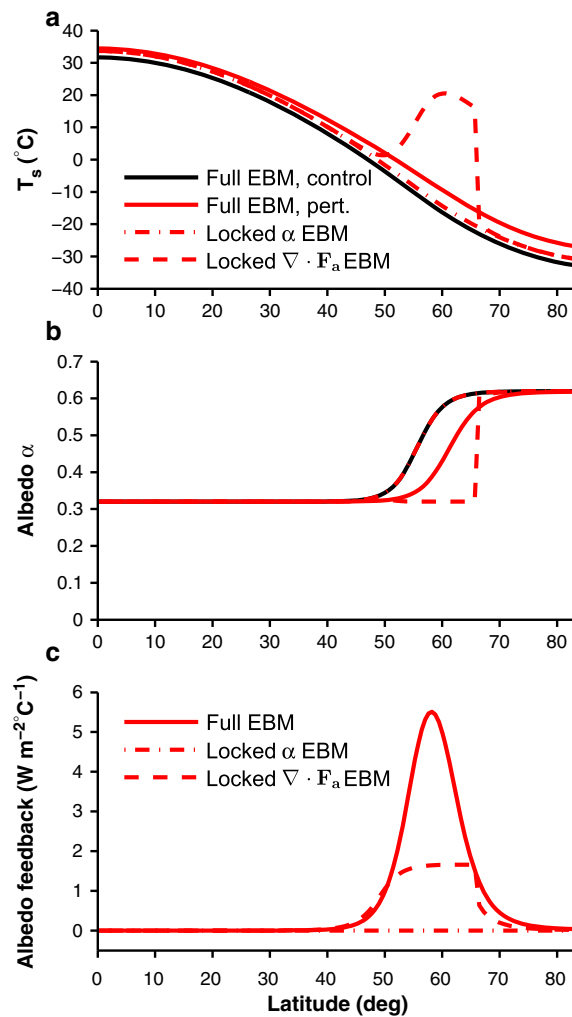
Figure 1. (a) Surface temperature and (b) surface albedo in the control (black) and perturbation (red) simulations for three EBM variants, as indicated in the legend. (c) Surface albedo feedback for three EBM variants, where the feedback is defined using the local surface temperature change: $\frac{1}{4}QS(\phi)\Delta\alpha(\phi) \times [\Delta T_s(\phi)]^{-1}$. The alternative of normalizing by the global-mean surface temperature change is shown in Figure S3 in the supporting information.

in (1). The control simulation has no radiative forcing ($\mathcal{F} = 0$ W m^{-2}), and the perturbation EBM simulations have a uniform radiative forcing of $\mathcal{F} = 3.5$ W m^{-2}.

Diffusion is discretized using a second-order finite difference scheme with 180 meridional grid points between the equator and pole spaced equally in x. The EBM is integrated to equilibrium using a fourth-order Runge-Kutta method from a uniform initial condition of 5°C for the control simulation and from the equilibrated temperature of the control simulation for the perturbation simulations. The results presented here are similar to those obtained with step function surface albedo temperature dependence, reduced radiative forcing amplitude, higher horizontal resolution, and an alternate time discretization.

Perturbation simulations ($\mathcal{F} = 3.5$ W m^{-2}) are performed with prescribed surface albedo from the control simulation, $\alpha(T_s|_{\text{REF}})$ and with prescribed convergence of the atmospheric energy transport from the control simulation, $\partial_x \left[D(1 - x^2)\partial_x T_s|_{\text{REF}} \right]$. The simulation with prescribed atmospheric energy transport is effectively a set of single-column model simulations that span all latitudes. The EBM simulations with locked processes are compared with inferences made from analyzing the perturbation TOA energy balance of the full EBM about regional surface temperature change.

The TOA energy balance surface temperature analysis (2) applied to the EBM takes the form

$$\Delta T_s(\phi) = \frac{-\mathcal{F} + \Delta \left[\nabla \cdot \mathbf{F_a}(\phi) \right] + \frac{1}{4}QS(\phi)\Delta\alpha(\phi)}{B}. \tag{5}$$

The right-hand side of (5) has contributions from the radiative forcing, change in divergence of the atmospheric energy transport, and surface albedo feedback, which are referred to as "components of the TOA energy balance surface temperature analysis" in what follows.

3. Results

3.1. Diffusive EBM Response to Radiative Forcing

Figure 1a shows the surface temperature for the control and radiatively forced simulations with interactive, temperature-dependent surface albedo and interactive atmospheric energy transport (solid lines). The warming is greater at high latitudes than low latitudes; the warming in the region from 60° to the pole is amplified relative to the global mean by about 50%. The "ice line" of the control simulation is near 60° and moves poleward with warming—this is a region of strongly positive surface albedo feedback (Figures 1b and 1c). The change atmospheric energy transport diverges energy from the region of perturbed surface albedo and converges it poleward and equatorward of that region (as can be inferred from Figure 2a).
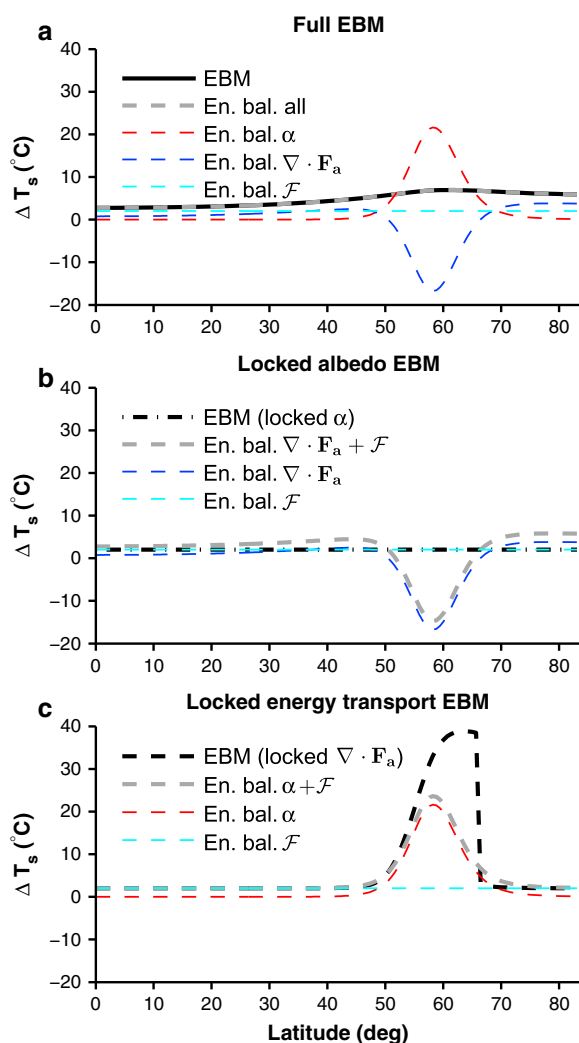
Figure 2. (a) Surface temperature change and components of the TOA energy balance surface temperature analysis (5) of the "full EBM" with interactive surface albedo and interactive atmospheric energy transport (colored dashed lines, labeled "En. bal.," are surface temperature changes in °C associated with individual components of the TOA energy balance, as indicated in the legend, and the gray dashed line is their sum). Surface temperature change (black) and expected surface temperature change from TOA energy balance analysis (gray) in locked simulations with (b) prescribed surface albedo and (c) prescribed atmospheric energy transport. In Figures 2b and 2c, the change in individual components of the TOA energy balance are taken from the full EBM.

The relationship between this and other components of the TOA energy balance in affecting the regional surface temperature response is examined in the next section.

When the surface albedo is locked (prescribed from the control simulation), the warming is uniform—there is no polar amplification (Figures 1a and 2b, dash-dotted line). This can be understood from the EBM's governing equation: with spatially uniform forcing $\mathcal{F}$ and no change in surface albedo, the surface temperature gradient and concomitant atmospheric energy transport are unchanged. Every latitude warms by exactly $-\mathcal{F}/B$, the feedback-free climate sensitivity.

When the surface albedo is interactive and the atmospheric energy transport is locked to that of the control simulation, the warming is dramatically amplified near 60° (Figure 1a, dashed line). The increase in absorbed solar radiation from the radiatively forced decrease in surface albedo can only be balanced by a *local* increase in outgoing longwave radiation.

3.2. TOA Energy Balance Surface Temperature Analysis

The TOA energy balance surface temperature analysis (5) accounts for the EBM-simulated temperature change (gray and black lines in Figure 2a). In addition to the uniform radiative forcing, the energy balance changes near 60° because of the decrease in surface albedo and the change in the divergence of the atmospheric energy transport. Poleward of the region of perturbed surface albedo, there is enhanced warming and an increase in the convergence of the atmospheric energy transport. Note that the pole has no surface albedo change. Likewise, equatorward of the region of surface albedo change there is more warming than that of the feedback-free climate sensitivity, which is consistent with an increase in the convergence of the atmospheric energy transport.

The EBM simulations with locked surface albedo feedback or atmospheric energy transport provide an interesting contrast to the inferences based on the TOA energy balance analysis of the full EBM. If one removes the effect of one of the changing components of the TOA energy balance, does it successfully capture the behavior of the EBM with that process locked? Figure 2b shows the result of the EBM simulation with locked surface albedo and compares it to the energy balance analysis with the surface albedo term removed: $\Delta T_s = B^{-1} \times \left[-\mathcal{F} + \Delta(\nabla \cdot \mathbf{F_a}) \right]$, where the change in atmospheric energy transport is taken from the full EBM simulation. As only the perturbation atmospheric energy transport has spatial variations, the TOA energy

Table 1. TOA Energy Balance Surface Temperature Analysis (5) of the Warming Poleward of 70° in Two EBM Variants That Differ Only in Surface Albedo Parameter Values[a]

Albedo Parameters		EBM	TOA Energy Balance (5)			
α_o		α_i	Polar ΔT_s	$\mathcal{F}$	$\Delta\alpha$	$\Delta(\nabla \cdot \mathbf{F}_a)$
0.32		0.62	6.2°C	2.0°C	0.5°C	3.6°C
0.33		0.60	5.7°C	2.2°C	0.3°C	3.2°C

[a]The global-mean surface temperature change is 8% larger for the standard parameters (top row), so all values in the altered parameter row of the table (bottom row) are adjusted by this factor to isolate differences in the regional warming pattern. The discrepancy between the sum of TOA energy balance terms and the EBM-simulated change arises from rounding to the nearest 0.1°C.

balance analysis suggests a pattern of response following this component: a large negative temperature anomaly near 60°, where the anomalous divergence of the atmospheric energy transport is large in the full EBM, and positive temperature anomalies poleward and equatorward of this region, where there is anomalous energy convergence in the full EBM (gray line in Figure 2b). However, the EBM with locked surface albedo has uniform warming ($-\mathcal{F}/B = 2$°C) and no change in atmospheric energy transport (black line in Figure 2b). In short, it is clear that the spatial structure of the divergence of the atmospheric energy transport is associated with the spatial structure of the surface albedo change in the EBM. So inferences based on removing one component of the energy balance in isolation do not account for simulations with locked components because the interactions between the changing components are important.

In the EBM simulation with locked atmospheric energy transport, the warming follows the feedback-free climate sensitivity $-\mathcal{F}/B$ in low latitudes and poleward of 70°, while the warming is substantial (≈ 40°C) near 60° (Figure 2c). This simulation exhibits hysteresis; another equilibrium solution, obtained from an ice-free isothermal initial condition, has a nearly ice-free pole. For the equilibrated temperature obtained from perturbing the control simulation temperature (shown in Figure 2), the TOA energy balance analysis successfully captures the behavior in low- and high-latitude regions where the albedo is unchanged and the warming follows the feedback-free sensitivity. Removing the perturbation convergence of the atmospheric energy transport from the high-latitude energy balance of the full EBM suggests the magnitude of the warming in the region of perturbed albedo would be ≈ 20°C (Figure 2c). In the locked energy transport EBM, the magnitude of the warming substantially exceeds this (≈ 40°C) and the magnitude of the albedo feedback is altered (Figure 1c). The magnitude of the warming is close to an upper bound given by the product of the high-latitude insolation (≈ 240 W m^{-2}) and the difference in surface albedo between ocean and ice ($= -0.3$ for the parameters here) divided by the longwave feedback parameter ($= -1.75$ W m^{-2} °C^{-1} here): $\Delta T_s \lesssim \frac{1}{4}QS(\alpha_o - \alpha_i) \times B^{-1}$. Taken together, the results of the locked EBM simulations show that the spatial structure of the feedbacks modulates the energy transport (Figure 2b) and that changes in the energy transport modulate the magnitude of the feedbacks (Figures 1c and 2c).

The nature of the interaction between the TOA energy budget components can be further isolated by replacing the nonlinear temperature dependence of the albedo (4) with a linear temperature dependence that is confined to a limited latitudinal range in the perturbation simulation. Simulations with this spatially confined *linear* feedback reproduce the results shown in Figures 1 and 2 (Figures S1 and S2). The key interaction—between spatially confined feedbacks and the nonlocality of the energy transport—would also exist if moist static energy was diffused rather than temperature [e.g., *Rose et al.*, 2014], though these EBMs differ in that they have polar amplification in the absence of the surface albedo feedback.

Beyond attributing regional changes to individual components of the TOA energy balance components, this analysis (2) has been used to interpret the role of individual processes in determining multimodel ensemble spread. However, the interactions between changing components of the energy balance suggests that uncertainty in one component of the energy balance may affect others. To illustrate this, the diffusive EBM with two formulations for the temperature-dependent surface albedo (4) are presented (all other parameters are identical). Table 1 shows the TOA energy balance analysis of the surface temperature change in the region poleward of 70°, normalized by the global-mean surface temperature change to emphasize differences in regional warming. (Differences in climate sensitivity between the full and locked simulations shown in Figure 2 could also be accounted for, but the spatial pattern of the warming is sufficiently distinct that it is clear such an adjustment would not substantially affect the discrepancies between the TOA energy balance surface temperature analysis (5) and the locked EBM simulations.) The highest latitudes are a region of small surface albedo change and, consistent with this choice of averaging region, the largest difference in the local TOA energy balance between the two EBMs is associated with energy transport (Table 1).

In this "perturbed physics ensemble" of EBMs, the only change in the model formulation is in the temperature dependence of the surface albedo. However, differences in the simulated climate are not limited to the region of perturbed surface albedo because the energy transport is nonlocal. An apparently substantial source of intermodel spread (the difference in energy transport) is arguably the nonlocal manifestation of the other source of intermodel spread (the difference in surface albedo arising from the perturbed model parameters), rather than being the underlying cause of the spread between the high-latitude warming in the two EBMs.

4. Discussion and Conclusions

The top-of-atmosphere (TOA) energy balance plays a fundamental role in the climate response to radiative forcing agents. The local form of the perturbation TOA energy balance is linear in its individual components (radiative forcing, divergence of energy transport, and radiative feedbacks), so it seems to offer a technique for quantitatively attributing regional surface temperature changes to these components. Here I have shown that interactions between components of the TOA energy balance lead to ambiguity in the meaning of such decompositions: when one component of the TOA energy balance is removed, the other components may change differently. The diffusive energy balance model (EBM) provides a clear illustration of these interactions—the changes in energy transport and spatially localized feedbacks are intertwined—that are concealed by the linearity of the TOA energy balance. The regional warming is *consistent* with fractional changes in the individual components of the local TOA energy balance (Figure 2a), though the EBM results show that this analysis cannot be used to determine the fraction of the regional warming that is *caused* by the changes in individual components (Figures 2b and 2c) and intermodel spread cannot be unambiguously attributed to individual processes (Table 1).

A key question is how relevant the diffusive EBM simulations are for understanding comprehensive models and Earth's climate system. Published results of GCM simulations with locked feedbacks provide useful context. The extent to which suppressing one feedback affects energy transport or other feedbacks gives an indication that the interactions found in the EBM also operate in GCM simulations of CO_2-forced climate change. Simulations using the GCM configuration of *Feldl and Roe* [2013] with locked surface albedo feedback have substantially different changes in the atmospheric energy transport response from those with interactive surface albedo feedback (N. Feldl, personal communication, 2014). *Schneider et al.* [1999] showed the results of simulations in which the free-tropospheric water vapor feedback is suppressed in different latitude bands. The spatial pattern of surface temperature change in these simulations provides clear evidence that the atmospheric energy transport interacts with the regional components of the water vapor feedback [*Schneider et al.*, 1999, Figure 5b]. *Mauritsen et al.* [2013] showed that the global-mean radiative feedbacks in feedback-locking simulations do not necessarily add linearly. For example, when the surface albedo feedback is locked, the global cloud feedback is more destabilizing, which the authors related to a dependence of the atmospheric circulation changes and local cloud feedbacks on the surface albedo [*Mauritsen et al.*, 2013, Figure 12]. *Graversen et al.* [2014] showed that the lapse rate feedback is more destabilizing in high latitudes when the surface albedo feedback is interactive than when it is locked. These GCM simulations with locked feedbacks suggest that the interactions between components of the TOA energy balance in EBM simulations are indeed relevant to more comprehensive climate models. On the other hand, GCM simulations with a different feedback-locking technique that corresponds closely to applying the individual radiative changes from the feedback terms on the right-hand side of (2) have regional surface temperature changes that add linearly [*Langen et al.*, 2012; *Mauritsen et al.*, 2013].

Here the results of EBM simulations with and without locked feedbacks have been compared to the TOA energy balance surface temperature analysis ((2) and (5)). Simulations with locked feedbacks may not be the definitive means for assessing the contribution of a given component of the energy balance to local response; they may have different sensitivities than the fully interactive system and may exaggerate the influence of components which are not locked. However, they provide a complementary perspective to the TOA energy balance surface temperature analysis: they allow for interactions between components of the energy balance, rather than providing a consistent description of the sum of simulated changes in the local TOA energy balance. In light of the EBM results presented here and the evidence offered by the aforementioned GCM feedback-locking simulations, a direct comparison of the expectations for the spatial pattern of warming based on the TOA energy balance analysis and GCM simulations with locked feedbacks would be instructive.

References

Alexeev, V. A., and C. H. Jackson (2013), Polar amplification: Is atmospheric heat transport important?, *Clim. Dyn.*, *41*, 533–547.

Crook, J. A., P. M. Forster, and N. Stuber (2011), Spatial patterns of modeled climate feedback and contributions to temperature response and polar amplification, *J. Clim.*, *24*, 3575–3592.

Feldl, N., and G. H. Roe (2013), The nonlinear and nonlocal nature of climate feedbacks, *J. Clim.*, *26*, 8289–8304.

Graversen, R. G., P. L. Langen, and T. Mauritsen (2014), Polar amplification in CCSM4: Contributions from the lapse rate and the surface albedo feedbacks, *J. Clim.*, *27*, 4433–4450.

Kay, J. E., M. M. Holland, C. M. Bitz, E. Blanchard-Wrigglesworth, A. Gettelman, A. Conley, and D. Bailey (2012), The influence of local feedbacks and northward heat transport on the equilibrium Arctic climate response to increased greenhouse gas forcing, *J. Clim.*, *25*, 5433–5450.

Langen, P. L., R. G. Graversen, and T. Mauritsen (2012), Separation of contributions from radiative feedbacks to polar amplification on an aquaplanet, *J. Clim.*, *25*, 3010–3024.

Lu, J., and M. Cai (2009), A new framework for isolating individual feedback processes in coupled general circulation climate models. Part I: Formulation, *Clim. Dyn.*, *32*, 873–885.

Mauritsen, T., R. G. Graversen, D. Klocke, P. L. Langen, B. Stevens, and L. Tomassini (2013), Climate feedback efficiency and synergy, *Clim. Dyn.*, 2539–2554.

North, G. R., R. F. Cahalan, and J. A. Coakley (1981), Energy balance climate models, *Rev. Geophys.*, *19*, 91–121.

Pithan, F., and T. Mauritsen (2014), Arctic amplification dominated by temperature feedbacks in contemporary climate models, *Nat. Geosci.*, *7*, 181–184.

Rose, B. E. J., K. C. Armour, D. S. Battisti, N. Feldl, and D. D. B. Koll (2014), The dependence of transient climate sensitivity and radiative feedbacks on the spatial pattern of ocean heat uptake, *Geophys. Res. Lett.*, *41*, 1071–1078, doi:10.1002/2013GL058955.

Schneider, E. K., B. P. Kirtman, and R. S. Lindzen (1999), Tropospheric water vapor and climate sensitivity, *J. Atmos. Sci.*, *56*, 1649–1658.

Sellers, W. D. (1969), A global climatic model based on the energy balance of the Earth-atmosphere system, *J. Appl. Meteorol.*, *8*, 392–400.

Taylor, P. C., M. Cai, A. Hu, J. Meehl, W. Washington, and G. J. Zhang (2013), A decomposition of feedback contributions to polar warming amplification, *J. Clim.*, *26*, 7023–7043.

Winton, M. (2006), Amplified Arctic climate change: What does surface albedo feedback have to do with it?, *Geophys. Res. Lett.*, *33*, L03701, doi:10.1029/2005GL025244.